The role of NO_2 and NO in the mechanism of hydrocarbon degradation leading to carbonaceous deposits in engines (supplementary information)

Radomir I. Slavchov[1,2*], Maurin Salamanca[2], Danilo Russo[2], Ibrahim Salama[3], Sebastian Mosbach[2], Stuart M. Clarke[3], Markus Kraft[2,4,5], Alexei A. Lapkin[2,5], Sorin V. Filip[6]

[1] *School of Engineering and Materials Science, Queen Mary University of London, Mile End Road, London E1 4NS, UK*
[2]*Department of Chemical Engineering, University of Cambridge, West Site, Philippa Fawcett Drive, Cambridge, CB3 0AS, UK*
[3]*BP Institute, University of Cambridge, Cambridge, CB3 0EZ, UK*
[4] *School of Chemical and Biomedical Engineering, Nanyang Technological University, 62 Nanyang Drive, Singapore 637459*
[5]*CARES – Cambridge Centre for Advanced Research and Education in Singapore, CREATE Tower, 1 CREATE Way, Singapore 138602*
[6] *BP Formulated Products Technology, Research and Innovation, Technology Centre, Pangbourne, UK*

**Corresponding author:* r.slavchov@qmul.ac.uk

S1. List of symbols and abbreviations

C_i	molar concentrations of *i* in the gas phase
F	feed volume rate
K_{H}^{CC}	Henry's constant, defined as ratio concentration in the liquid/concentration in the gas
k	rate constant
p	pressure in the autoclave
R	gas constant
r_{i}	initiation rate
T	temperature
t	time
V	volume of the autoclave
V^{G}	volume of the gas phase
V^{L}	volume of the liquid phase
x_{i0}	mole fraction of *i* in the gas phase before it is introduced in the autoclave
x_{C8}	mole fraction of the isooctane in the gas phase
τ	mean residence time
C1	methyl
C3	2-propyl
C4	methyl-2-propyl
C5	dimethyl-1-propyl

$C7_2$ 2,4-dimethyl-2-pentyl
$C7_4$ 4,4-dimethyl-2-pentyl
$C8_1$ 2,2,4-trimethyl-1-pentyl
$C8_3$ 2,2,4-trimethyl-3-pentyl
$C8_4$ 2,4,4-trimethyl-2-pentyl
$C8_5$ 2,4,4-trimethyl-1-pentyl

aH abstraction of hydrogen by a radical
C_1o oxidation of primary alkyls with formation of aldehydes
C_2o oxidation of secondary alkyls with formation of ketones
o oxidation of alkyl
R_3O_2 process of rearrangement of tertiary alkyl peroxy radicals with transfer of an alkyl group
β β-scission process

ppm molar parts per million

{O_2;*T*}, {O_2;*T*,Sc}, {NO_2;*T*}, {NO_2;*C*}, {NO;*T*}, {NO;*C*}, {NO_2+NO}, {NO_2+NO;Sc}: codes to the eight experiments performed, as specified in Table 2. O_2 stands for "oxygen only", i.e. nitrogen oxides are absent. Sc stands for radical scavenger in the liquid phase. NO and NO_2 mean that these gases were present in the gas feed. Note that NO_2 was present in the autoclave in tests {NO;*T*} and {NO;*C*}, due to the reaction (4); in contrast, no significant quantity of NO is expected to appear in {NO_2;*T*} or {NO_2;*C*}. *T* stands for variable temperature; *C* stands for variable concentration of the NO_x during the experiment.

S2. Flammability limits and autoignition

Available data for the limits of flammability of isooctane as a function of the temperature *T*, at 1 atm, are summarized in the following table:

	x_{LL}, lower limit of flammability, 1 atm, *x*%	x_{UL}, upper limit of flammability, 1 atm, *x*%
26 °C	1.03 [a] [35]	
100 °C	0.96 [a] [35]	
150 °C	0.91 [a] [35]	
200 °C	0.88 [a] [35]	
60°C	0.77 [b]	6.1 [c]
100 °C	0.74 [b]	6.3 [c]
150 °C	0.71 [b]	6.5 [c]
200 °C	0.68 [b]	6.7 [c]
room temperature	0.98 [37]	6.03 [37]
24 °C	0.8 [39]	
60 °C		5.9 [39]

[a] Extrapolation of the data from Ref. [35] to x_{LL} = 0 % gives 1200 °C for the flame temperature (close to the expected 1300 °C [36], confirming the reliability of the data). [b] Extrapolated values under the assumption that the flame temperature is 1300 °C [36]. [c] Extrapolated values using the modified Burgess-Wheeler law of Zabetakis, *eq 37* in Ref. [36], $x_{UL}/x_{UL,25\,°C}$ = 1+0.000721(T(°C)-25).

Further, we use the worst case scenario from the values in this table, namely x_{LL} = 0.8 % and x_{UL} = 6 % at room temperature, corresponding to 0.71 % and 6.5% at 150 °C, respectively, based on the correlations of Zabetakis [36].

We further correct these limits for the pressure dependence. To do so, we use the pressure dependence of natural gas (90% methane + 10% ethane) – its flammability limits depend on pressure as $x_{LL}/\% = 4.9 - 0.71\times\lg(p/\text{atm})$ for the lower limit and $14.1+20.4\times\lg(p/\text{atm})$ for the upper limit (*fig 26* and *eqs 41-42* in Ref. [36]). We assume that the pressure factor multiplying the ratio fuel/O_2 at the lower and the upper limits is similar for different fuels, given by

$$4.0757\times[0.049 - 0.0030835\times\ln(p/\text{atm})]/[0.19971 + 0.0006475\times\ln(p/\text{atm})] \text{ and}$$

$$1.27936\times[0.141 + 0.088596\times\ln(p/\text{atm}))/(0.18039 - 0.018605\times\ln(p/\text{atm})], \text{ respectively.}$$

We multiply the upper and the lower limits of isooctane+air by these ratios, and then recalculate from them the respective x_{LL} and x_{UL} at the increased pressure. The pressure has little effect on the lower limit (0.58 % isooctane at 15 atm vs. 0.71 % at 1 atm, 150 °C), but it has a significant effect on the upper one (21% isooctane at 15 atm vs. 6.5 % at 1 atm, 150 °C).

We finally construct the flame stability diagram upon dilution with N_2 of a mixture of isooctane and air. To do so, we use the fact that the diagram is close to triangular, the lower limit is nearly independent of the added N_2, and one of the edges of the triangle ("cusp") occurs near the stoichiometric mixture at the lower limit – this is illustrated in Figure 10.

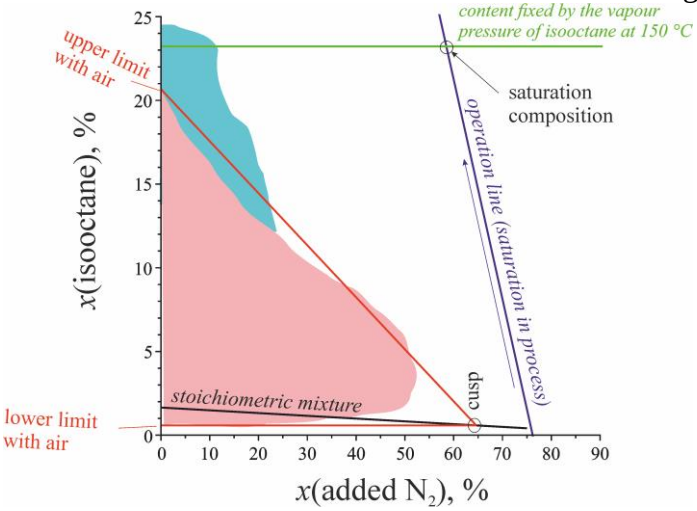

Figure 10. Flammability diagram for isooctane-nitrogen-oxygen mixtures – estimated flammability zone (red). Blue: rough estimate for the cool flame region. Green line: saturated isooctane vapour. Operation line: predicted conditions inside a gas bubble from entrance into the reactor (when x_{C8} = 0) until saturation with isooctane vapour.

The real flammability zone is always covering a smaller area than the triangle (as schematically illustrated with the red zone). The cool flame zone is expected to be outside it (the blue shape in the figure) but no occurrence of cool flame should be expected at dilutions above 30%. The shapes of the coloured areas are based on those of various well-studied paraffins [36].

The vapour pressure of isooctane at 150 °C was calculated using the monomer-dimer Clausius-Clapeyron formula from Ref. [31].We work with O_2:N_2 = 5:95. As the gas is bubbled through the isooctane, it will be diluted with isooctane vapours until it reaches saturation at 150 °C. This is not an instantaneous process, so the gas bubbles in the apparatus are expected to have all compositions from 0 to saturated concentration. These compositions correspond to the purple line in the figure (the operation line; the dilution of the N_2-O_2 mixture with isooctane vapours is taken into account). The gas composition, as seen, is expected to fall outside the flammability region under all conditions.

We also calculated the autoignition *T* of isooctane. At normal pressure, it is 683-720 K [40], and depends somewhat on the surface of the container. The autoignition *T* decreases with

the increase in pressure. Judging from the data for 0.82 isooctane + 0.18 hexene (stoichiometric mixture, at 150 ms autoignition time), the increase in pressure leads to fall in the autoignition temperature by 5 $K \cdot atm^{-1}$ (in the range 10-13 bar), which is roughly 610-645 K at 15 bar. Then, another extrapolation to autoignition time of 3 s (using Semenev's formula with activation energy of 110 $kJ \cdot mol^{-1}$) gives 550 K, or 277 °C. This is well above the studied temperature range. Another check of this estimate was done as follows: the autoignition temperature of isooctane (average chain length of 4.2) should be expected to be between those of butane (400 °C at increased pressure) and pentane (300 °C). An additional factor is the fact that we are not working with stoichiometric mixtures: this is going to raise the autoignition temperature significantly.

S3. Toxicity of NO and NO_2

The immediately-dangerous-to-life-and-health (IDLH) concentration (as specified by the National Institute for Occupational Safety and Health) of NO is 100 ppm, and of NO_2 – 20 ppm. The concentrations and the amounts of NO and NO_2 in the three cylinders were chosen to be small enough that even the simultaneous discharge of all three cylinders in the laboratory space would result in concentrations well below IDLH. As an additional safety measure, we installed MultiRAE with sensors for NO and NO_2 to monitor for leaks.

The experiments were conducted in a safety cabinet equipped with fume extractor to remove any gas/liquid vapour residues. Under the most severe experimental conditions, the concentrations of NO and NO_2 in the autoclave are 100 ppm NO_2 + 500 ppm NO in 130 mL autoclave. After each experiment, 25-30 L N_2 was blown through the autoclave to evacuate the NO_x safely.

S4. Additional results and experimental data

In Figure 11, we list all the perhydroxy alkyl radicals that can be produced from the key ten alkyl peroxy radicals $RO_2\cdot$, where R is one of the alkyls from the list (3). These are not of equal concentrations: the tertiary radicals are more stable, and those in which the H-O-O-C-…-C· sequence is 5 or 6 atoms long are more likely to appear [38]. There is a list of respective hydroxy alkyl radicals that differ by a -OH instead of $-O_2H$ group; these are not as selective with respect to the tertiary position of the missing hydrogen atom, and those in which the H-O-C-…-C· sequence is 5 or 6 atoms long are more likely to appear [38]. However, the hydroxy alkyl radicals are thought to be more prone to β-scission reactions than to intramolecular hydrogen abstraction [44].

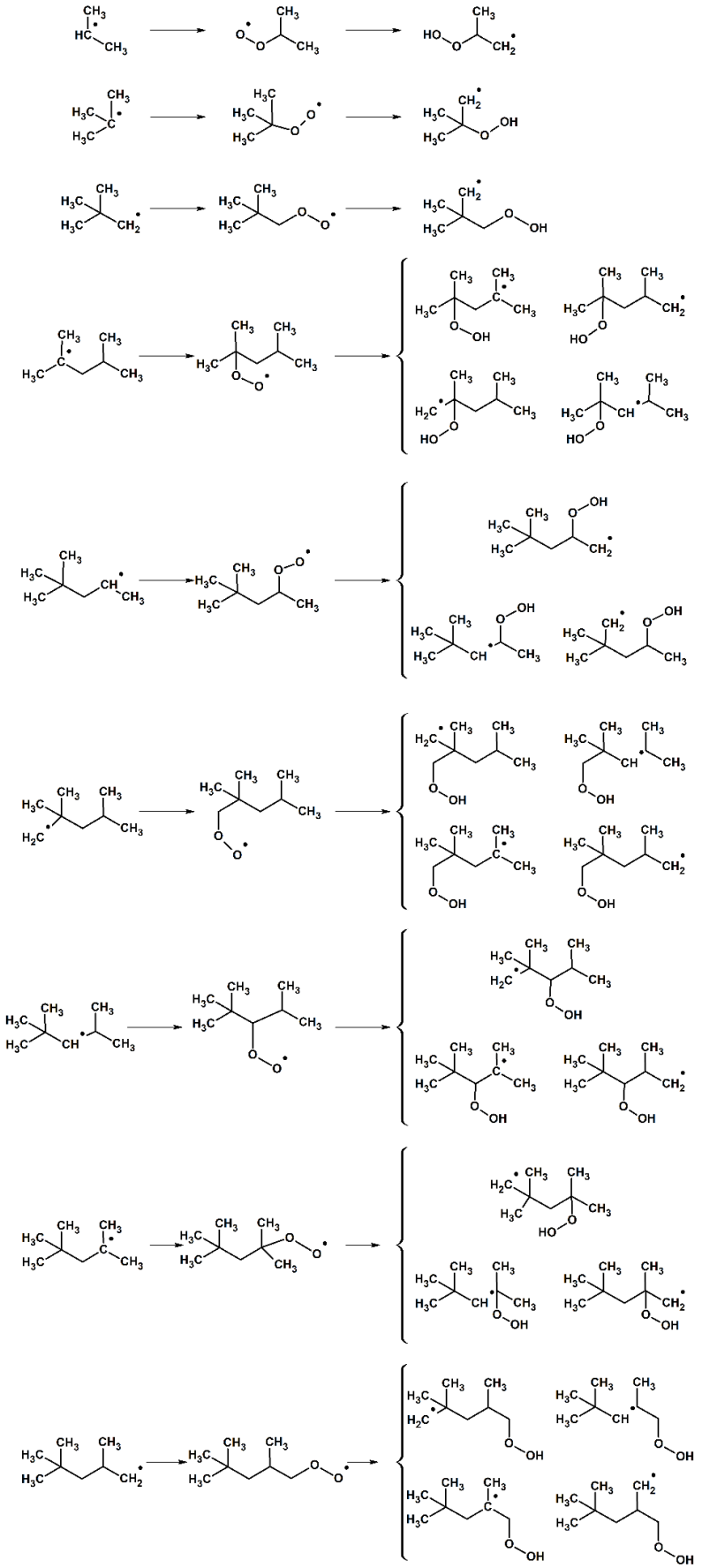

Figure 11. Key perhydroxy alkyl radicals produced by the nitro-oxidation of isooctane.

The concentrations of the four isomers of isooctanol ($C8_xOH$, x = 1,3,4,5) in tests {NO;*T*} and {NO_2;*T*} are given in Figure 12a; let us remind that only $C8_4OH$ has been calibrated, and for the other three alcohols the same calibration curve has been used, as a rough approximation. Similarly, the concentrations of $C8_xOH$ in tests {NO_2+NO} and {NO_2+NO;Sc} are plotted in Figure 12b.

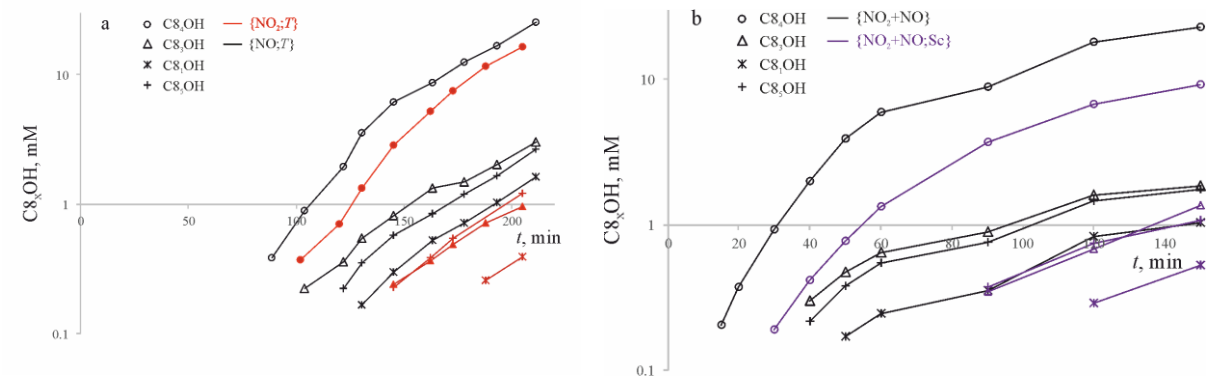

Figure 12. Concentration of the isomers of isooctanol ($C8_1OH$, $C8_3OH$, $C8_4OH$, $C8_5OH$) (a) in tests {NO_2;*T*} and {NO;T}; (b) in tests {NO_2+NO} and {NO_2+NO;Sc}. Only [$C8_4OH$] has been calibrated against the GC-MS signal – the other three concentrations are estimates only.

To compare the relative amounts of various products in tests {NO_2;*T*} than in {NO;*T*}, we used the values of the relative selectivity defined as:

$$S_i^T = \frac{area_i^{\{NO_2;T\}}}{area_i^{\{NO;T\}}} \times \frac{area_{C8_4OH}^{\{NO;T\}}}{area_{C8_4OH}^{\{NO_2;T\}}}. \qquad (13)$$

Here, $area_i^{\{\ldots\}}$ stands for the area of the MS peak for compound *i* in test {…}, as determined in the last probe taken. A value of $S_i^T > 1$ means that a higher proportion of compound *i* is formed in {NO_2;*T*} than in {NO;*T*}, relative to $C8_4OH$, i.e. without NO *relatively* more *i* is produced. The selectivities S_i^C and S_i^{Sc} are similarly defined:

$$S_i^C = \frac{area_i^{\{NO_2;C\}}}{area_i^{\{NO;C\}}} \times \frac{area_{C8_4OH}^{\{NO;C\}}}{area_{C8_4OH}^{\{NO_2;C\}}}; \qquad (14)$$

$$S_i^{Sc} = \frac{area_i^{\{NO_2+NO;Sc\}}}{area_i^{\{NO_2+NO\}}} \times \frac{area_{C8_4OH}^{\{NO_2+NO\}}}{area_{C8_4OH}^{\{NO_2+NO;Sc\}}}. \qquad (15)$$

The values of the selectivities for several products are listed in Table 3. The selectivity shift in the presence of NO is also illustrated also by the comparison of the chromatograms for tests {NO_2;*T*} and {NO;*T*} in Figure 2.

Table 3. Difference between the detected oxidation products in NO-nitro-oxidation and NO_2-nitro-oxidation.

	[a] S_i^T {NO_2;*T*}:{NO;*T*}	[b] S_i^C {NO_2;*C*}:{NO;*C*}	[c] S_i^{Sc} {NO_2+NO;Sc}:{NO_2+NO}
$C8_4OH$	1	1	1
$C8_3OH$	0.48	0.8	1.5
$C8_1OH$	0.35	0	1.02
$C8_5OH$	0.67	1.19	1.24
acetone	0.97	1	0.84
tert-butanol, C4OH	1.51	0.62	0.52
2,4,4-trimethyl-1-pentene	1.07	2.03	2.06
2,4,4-trimethyl-2-pentene	1.44	2.18	3.38
2,2-dimethyl-1-propanol nitrate	<<1	[e]	>>1
2,2,4-trimethyl-4-nitropentane	<<1	[e]	1.23
2-nitro-*tert*-butanol	<<1	[e]	1.67
dimethylpropanal	[d] 1.49	[e]	<<1
2-methyl propionic acid	[d] 1.41	[d] 1.34	0.57
2,2-dimethylpropionic acid	[d] 1.59	[e]	1.74
3,3-dimethyl-butanoic acid	[d] 3.49	[d] 3.79	0.51
2,2,4-trimethyl-1,3-pentanediol	0	[e]	[e]
2,4-dimethyl-2,4-pentanediol	0.87	0.84	0.53
tetrahydro-2,2,4,4-tetramethylfuran	0.99	2.07	>>1
2-dimethylethyl-3-methyloxetane	0.82	<<1	0.83

[a] Calculated through Eq (13); if $S_i^T > 1$, then more *i* is formed in {NO_2;*T*} than in {NO;*T*}, relative to $C8_4OH$. [b] Eq(14); if $S_i^C > 1$, then more *i* is formed in {NO_2;*C*} than in {NO;*C*}, relative to $C8_4OH$. [c] Eq (15); if $S_i^{Sc} > 1$, then more *i* is formed in {NO_2+NO;Sc} than in {NO_2+NO}, relative to $C8_4OH$. [d] These compounds have $S_i > 1$ close to the end of the respective two tests, but $S_i < 1$ before that (behaviour like C4OH in Figure 4c). [e] Signal(s) not strong enough to evaluate the selectivities.

Figure 13 is an example for the evolution with time and temperature of the chromatographic peak of one of the major products, $C8_4OH$, in test {NO_2;*T*}. No significant signal has been detected at temperatures lower than 140 °C. In all cases, no significant asymmetry of the peaks has been observed. The areas of the peaks were used to quantify the concentration of $C8_4OH$, Figure 4a, using a calibration curve (eleven solutions of $C8_4OH$ in isooctane, 6-50 mM).

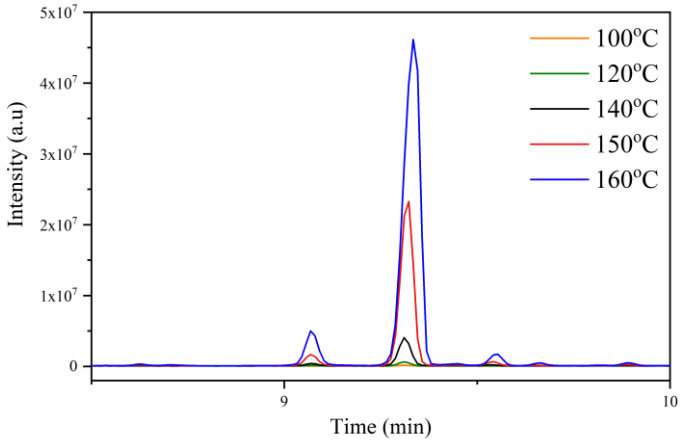

Figure 13. Evolution of the chromatographic peak of $C8_4OH$ with the advance of test {NO_2;*T*}; each curve corresponds to the GC-MS signal for the samples taken 30 min after the indicated temperature has been reached (cf. Figure 4 for the relation between time and temperature).